Swiss Accelerator Research and Technology

CHART Scientific Report

Prototypes and proofs of principle for critical FCC-ee injector components and definition of the technical system interfaces for linacs, electron and positron sources

FCC-ee Injector linacs and sources

PSI:

P. Craievich, F. Addesa, B. Auchmann, I. M. Besana, S. Bettoni, M. Duda, R. Fortunati, A. Foskolos, M. Gloor, D. Hauenstein, R. Ischebeck, P. Juranic, J. Kosse, T. G. Lucas, U Michlmayr, G. L. Orlandi, J.-Y. Raguin, N. Strohmaier, D. Stephan, C. Vicario, R. Ganter, M. Zykova, R. Zennaro

CERN:

A. Grudiev, S. Doebert, J. L. Grenard, E. Granados, G. Tenasini, R. Rossel, A. Omoumi, A. Kurtulus, A. Latina, R. Mena Andrade, A. Perillo Marcone, Z. Vostrel

CNRS-IJCLab:

I. Chaikovska, V. Mytrochenko, Y. Wang

INFN-LNF:

C. Milardi, A. De Santis

30 April 2026

1 Introduction/Original goals of the project

This report presents an overview of the progress and results achieved within the collaboration on the FCC-ee injector study within the CHART 2025-2028 programme. The collaboration brings together PSI and CERN, along with key external partners, including CNRS-IJCLab (Orsay, France) and INFN-LNF (Frascati, Italy). Additional contributions are provided by KEK (Tsukuba, Japan), which participates as an external observer and consultant for the P^3 project, and by SLAC, which supports specific technical aspects of the injector complex and contributes to the experimental programme at FACET II. The project encompasses a set of well-defined deliverables, as outlined in CHART/PR/20.

The expected results of the project can be grouped into two main areas. The first concerns

beam physics studies aimed at finalising the injector baseline, enabling integration studies at the CERN site and the subsequent launch of civil engineering activities. A key outcome of this effort will be the preparation of the Reference Design Report, marking the transition to the Technical Design phase. The second area focuses on the development and testing of critical hardware components, including RF prototypes and the positron and electron sources, with the objective of addressing key challenges identified during the feasibility study phase and mitigating potential risks to the project implementation.

2 Realization

The CHART FCC-ee linacs and sources project is organised into six dedicated work packages (WPs), each focusing on a specific technical domain:

- WP0: Coordination of beam physics studies and experimental activities.
- WP1: Electron and high-energy (HE) linacs, including accelerating structures for the positron linac.
- WP2: Electron source.
- WP3: Positron linac, including beam dynamics, target system, and the P^3 experiment.
- WP4: Damping ring and transfer lines.
- WP5: Preparatory phase for the Technical Design Report.

The following chapters present an overview of the progress achieved within each work package, together with a summary of the main results obtained.

WP1: Electron and HE Linacs – Summary of Activities and Results

The work carried out in WP1 focused on the optimization of the high-energy (HE) linac, with particular emphasis on transverse single- and multi-bunch dynamics, RF structure design, and longitudinal beam manipulation through energy and bunch compressors. Extensive simulation studies were performed to identify a configuration capable of meeting the stringent requirements on emittance preservation and beam trajectory stability. Among the RF frequency options investigated, the 3 GHz solution was selected as baseline, as the 6 GHz option is incompatible with the present energy compressor design and machine layout.

(Single bunch) transverse static effects. The transverse beam dynamics of the HE linac have been investigated to verify compliance with the stringent emittance requirements at booster injection. The normalized emittances at the damping ring exit were assumed to be 10 mm mrad and 1 mm mrad in the horizontal and vertical planes, respectively. The corresponding maximum tolerated values at the booster injection are 20 mm mrad and 2 mm mrad. Since the vertical plane is more critical, the optimization was primarily focused on the normalized vertical emittance, while the horizontal plane was evaluated only after the final lattice had been selected.

A campaign of detailed simulation was performed using RF-Track [1]. Random lattice misalignments were included in the simulations to assess the impact of static imperfections. Gaussian-distributed alignment errors with rms values of 100 µm were assumed for quadrupoles and RF structures, and 30 µm for BPMs in both transverse planes, consistent with operational experience at SwissFEL. A conservative BPM resolution of 30 µm was also included.
For each configuration, 200 seeds were simulated. The final emittance was defined as the value below which 90% of the seeds fall. For each seed, the orbit was corrected using three steering algorithms applied in cascade: response-matrix-based correction, dispersion-free steering (DFS), and wakefield-free steering (WFS). Although WFS has been experimentally validated [6], in this study only response-matrix correction and DFS were used to provide a conservative estimate based on well-established techniques. The potential improvement from WFS is discussed separately. An example of the emittance distribution at the HE linac exit is shown in Fig. 1. The

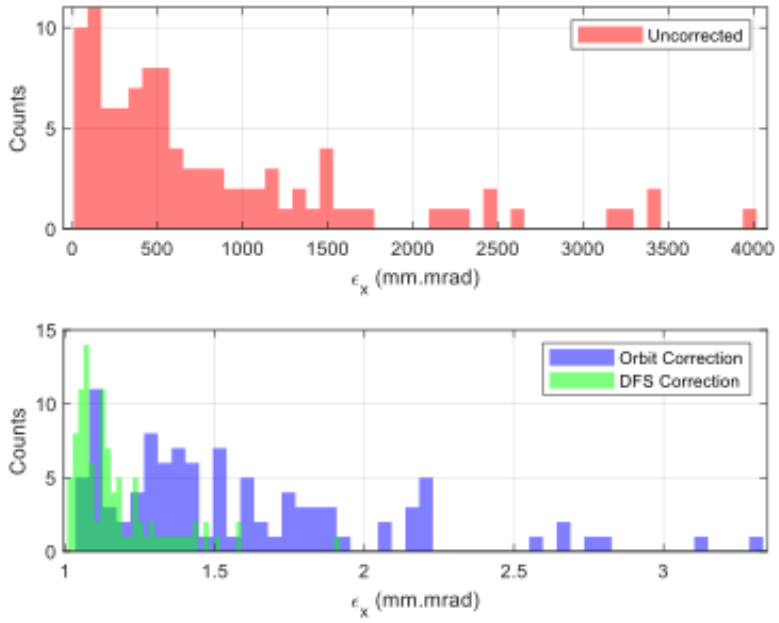

Figure 1: Emittance distribution at the end of the HE linac. Top plot: before any correction is applied. Lower plot: after the RM-based correction before and the DFS after have been applied.

threshold used to define the final emittance was changed from 98% to 90%, in order to reduce sensitivity to the tails of the distribution and ensure consistency with other projects.
The main optimization parameters were the RF aperture, expressed as a/λ (where a is the iris radius and λ the RF periodicity), the RF structure length, the phase advance per cell, and the number of quadrupoles per RF structure. The aperture mainly affects the transverse wakefields, while the other parameters determine the focusing strength and the beam optics.
As already pointed out in previous studies [5], the number of subsections (bins) used in the simulations is an important parameter. Also the change in the emittance threshold affects the optimum number of bins and has an impact of about 0.2 mm mrad on the final emittance, whereas doubling the quadrupole rms misalignment has only a marginal effect, as shown in Table 1.

Table 1: Final normalized emittance as a function of the number of subsections for different rms quadrupole alignment errors and evaluation thresholds in percentage. The minimum value in each row is highlighted in bold.

Bins $\longrightarrow$	**4**	**6**	**8**	**10**	**11**	**12**	**13**	**14**
ε_n, $\sigma_Q = 50\,\mu$m, 98%	64.99	–	1.80	1.49	–	**1.38**	–	1.41
ε_n, $\sigma_Q = 100\,\mu$m, 98%	245.11	7.92	2.56	1.96	1.51	1.45	1.42	**1.41**
ε_n , $\sigma_Q = 100\,\mu$m, 90%	147.05	6.0931	2.27	1.48	1.28	**1.21**	1.2403	1.30

The final selection was made in conjunction with the dynamic effects discussed in the next section.

(Single bunch) transverse dynamic effects. Dynamic effects were quantified through the jitter amplification (JA), defined as the square root of the ratio between the area transverse phase-space and defined by N bunches launched with different initial positions and angles and traveling through the HE linac. A complete description of the method can be found in Ref. [7]. Since no tolerances have yet been defined for the transfer line to the booster, a maximum acceptable JA of 2 was adopted based on the booster injection specifications. The design goal was not only to remain below this limit, but also to minimize the JA at the end of the HE linac at the first phase of the design and along it in the final stage of the study.

For all configurations considered, the final JA at the linac exit is lower than the incoming value, indicating intrinsic damping of orbit errors. In the selected operating conditions, the HE linac reduces incoming position and angle jitter by approximately one third, as shown in Fig. 2.

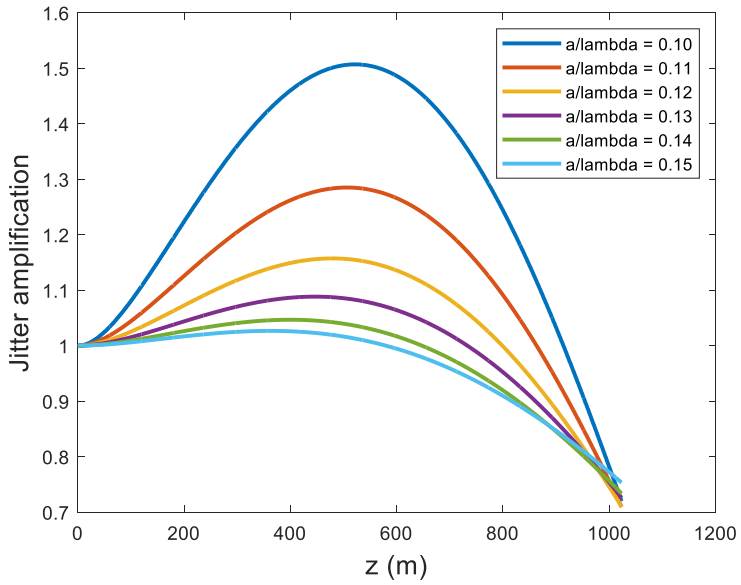

Figure 2: JA along the HE linac at different apertures of the RF structures.

In addition to the baseline lattice with one quadrupole per RF structure (2Q2RF), an alternative lattice with one quadrupole every two RF structures (1Q2RF) was also investigated. The 2Q2RF lattice provides smaller beam size and shorter betatron wavelength, at the cost of higher quadrupole strength, whereas the 1Q2RF lattice features larger beam size and weaker focusing. The 1Q2RF option was found to be less favorable in terms of JA over the parameter range considered. A systematic scan of RF structure length, RF aperture, and phase advance per cell

showed that shorter RF structures and larger phase advances generally improve JA performance. Shorter RF structures reduce the FODO cell length and increase the focusing, leading to lower final JA. Similarly, increasing the phase advance per cell reduces the beam size and results in improved JA. Figure 3 shows the dependence of JA on all the parameters combined.

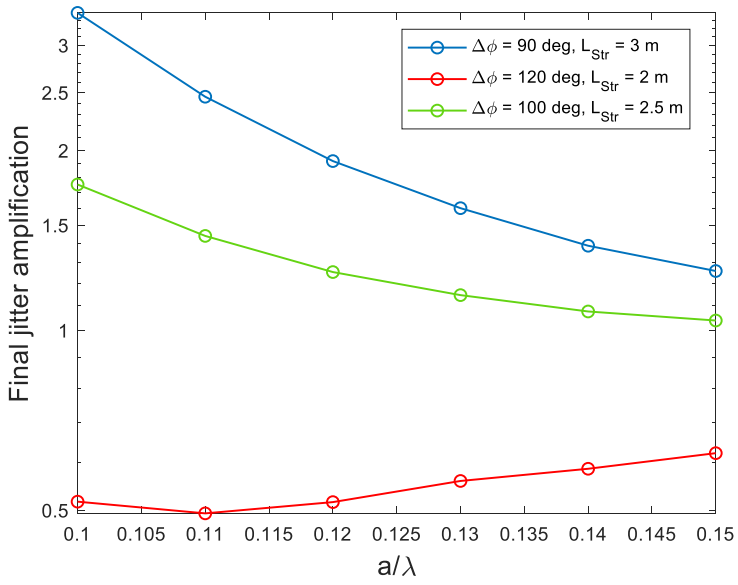

Figure 3: JA at the end of the HE linac assuming different phase advance per cell and RF structure lengths varying the Rf structure aperture.

The lowest final JA was obtained for configurations with short RF structures and large phase advance. However the final selection was therefore based on a compromise between transverse stability, emittance growth, RF performance, and cost, as discussed in the next section.

Selected HE-linac configurations. We summarize the most promising HE linac configurations, reporting the final emittance assuming an initial normalized vertical emittance of 1 mm mrad at the damping ring exit. For each case, the number of subsections (bins) was scanned and the configuration yielding the minimum emittance was selected. Only response-matrix-based orbit correction and DFS were considered, in order to provide a conservative estimate based on well-established techniques. Wakefield-free steering (WFS) is expected to further reduce the emittance by about 0.1–0.15 mm mrad, depending on the specific configuration. Table 2 summarizes the most promising configurations.

A compromise between beam dynamics performance, RF efficiency, and overall system complexity was selected. The present baseline corresponds to the cases indicated in bold in the table 2. The sensitivity to the initial emittance was investigated, showing that the emittance growth is approximately additive within a 20% accuracy. The final emittance can therefore be estimated by adding the computed growth to any updated initial value within this uncertainty. The analysis focuses on the vertical emittance, which has a tighter budget, while additional simulations with asymmetric initial emittances confirm similar relative growth in the horizontal plane with sufficient margin.

Overall, the proposed HE linac design fulfills all static and dynamic beam dynamics requirements with significant margin, allowing tolerance to possible variations in the initial beam parameters.

Table 2: Configurations simulated for the HE linac. Colors indicate performance ranges: green (emittance $<$ 1.5 mm·mrad, $JA_{max} < 1.2$, $JA_{Final} < 1.0$), yellow (emittance $<$ 1.6 mm·mrad, $JA_{max} < 1.5$, $JA_{Final} < 1.2$), and orange (emittance $>$ 1.8 mm·mrad, $JA_{max} > 1.8$). For space reasons we excluded from the table all the configurations giving results outside of any of the listed color code. Configurations with summed L_{str} correspond to the 1Q2RF scheme; all others correspond to 2Q2RF. Values are indicative, since the RF gradient is preliminary.

a/λ	L_{str} **m**	$\Delta\phi$ **deg**	ϵ **mm mrad**	N_{quad}	N_{struct}	N_{bpm}	**Linac length, m**	**Max JA**	**Final JA**	R_{eff} Ω
0.13	2.5	90	1.20	337	336	339	1111.5	1.03	0.25	93.1
0.13	3	90	1.22	281	280	283	1049.5	¡1.10	0.73	97.1
0.13	**3**	**80**	**1.19**	**281**	**280**	**283**	**1049.5**	**1.10**	**0.91**	**97.1**
0.13	3	70	1.20	281	280	283	1049.5	1.13	1.08	97.1
0.12	**3**	**90**	**1.46**	**283**	**282**	**285**	**1077.0**	**1.15**	**0.71**	**108**
0.12	3	80	1.36	283	282	285	1077.0	1.20	0.95	108
0.12	3	70	1.35	283	282	285	1077.0	1.26	1.17	108
0.13	4	90	1.48	211	210	213	1017.0	1.22	1.19	103.3
0.13	2+2	90	1.20	211	420	633	1069.5	1.21	1.12	103.3
0.13	2+2	100	1.17	211	420	633	1069.5	1.17	0.97	103.3
0.13	2+2	120	1.16	211	420	633	1069.5	1.13	0.56	103.3
0.12	2+2	100	1.28	212	422	636	1074.5	1.29	1.03	110.4
0.12	2+2	120	1.43	212	422	636	1074.5	1.22	0.52	110.4
0.13	2.5+2.5	120	1.26	169	336	505	1017.5	1.26	0.98	93.1
0.12	2.5+2.5	120	1.44	170	338	508	1023.5	1.42	1.06	104
0.13	3+3	90	1.34	–	–	–	–	1.60	1.60	97.1

This design was used to drive the RF design of the structures [8].

Collaboration with SLAC/FACET-II. An important aspect of the linac design is the amplification and damping of transverse beam jitter originating from upstream sections. To experimentally verify the damping mechanism observed in simulations, we recently carried out dedicated measurements at the FACET-II facility at SLAC. A schematic layout of the facility is shown in Fig. 4.

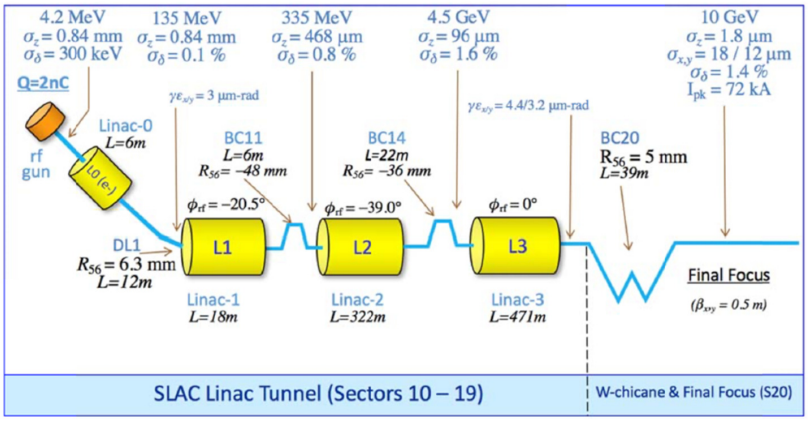

Figure 4: FACET-II schematic layout.

To perform these measurements, we implemented a "superknob" composed of two orbit correctors separated by a phase advance of 90 degrees, allowing a two-dimensional painting of the transverse phase space. Controlled orbit oscillations were generated by varying the strengths of the two correctors according to sine and cosine functions, and the evolution of the centroid phase-space area was measured along the linac.

Because the FACET-II linac is relatively shorter than the FCCee HE linac, it does not natu-

rally exhibit strong damping of transverse jitter amplification. The machine parameters were therefore optimized to enhance the visibility of this effect within the available lattice length by varying the bunch charge and bunch length. At each charge, the bunch was longitudinally decompressed at BC14 by adjusting the phase of Linac 2 (L2), thereby increasing the energy spread and enhancing the damping of transverse jitter. Linac 3 (L3) was operated on-crest, similarly to the high-energy linac in FCC-ee. The analysis is still ongoing, as the measurements were performed only very recently. Nevertheless, Fig. 5 shows BPM readings along the linac for several consecutive BPM pairs, for different bunch charges and L2 phase settings. Since the

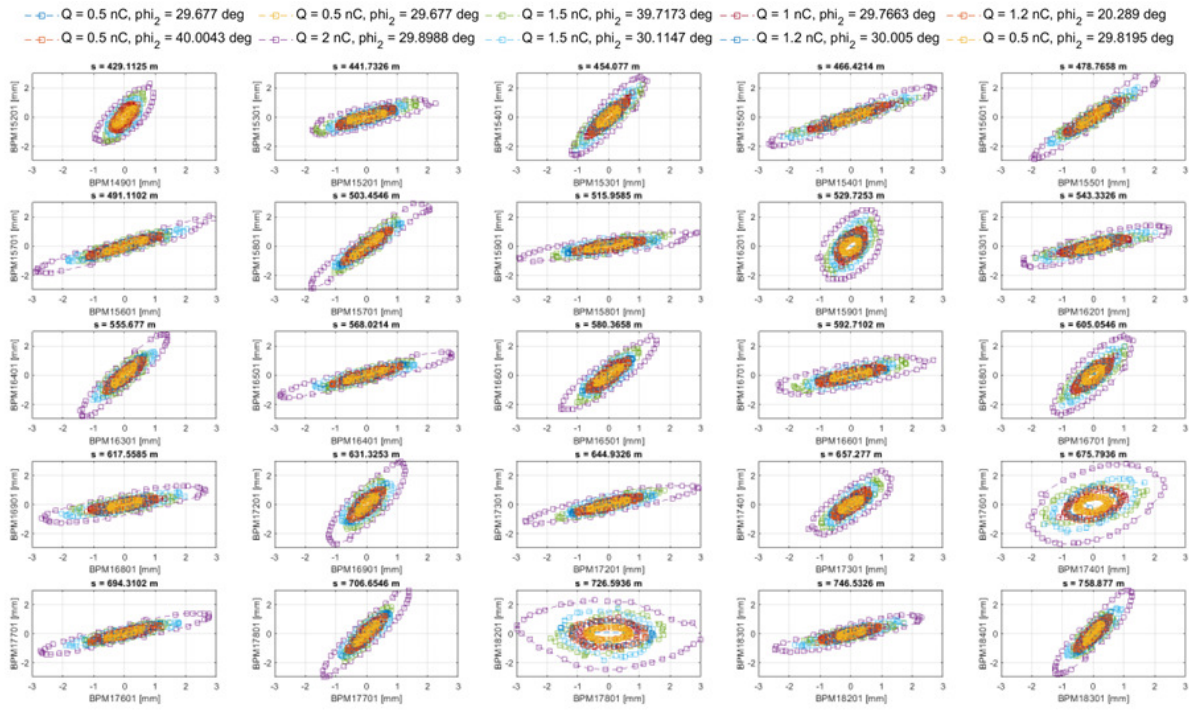

Figure 5: BPM pairs readings along the FACET-II linac for different operating conditions. The configurations shown are listed in the legend.

FACET-II model is known to exhibit discrepancies with respect to the actual machine in the low energy section, the area of each ellipse was normalized to that of a reference case corresponding to a charge and L2 phase with an approximately flat jitter evolution to reduce the dependence of the results on the optics. An effort is currently underway to reconstruct the optics directly from measured data. Figure 6 shows the evolution of the normalized area along the machine for the most relevant operating configurations. Simulations performed in preparation for these measurements indicate that optimal conditions for observing damping of transverse jitter amplification correspond to a bunch charge in the range 1–1.5 nC and an L2 phase of approximately 40 degrees. These preliminary results appear consistent with the measurements, although further analysis is ongoing and additional measurements are planned.

FACET-II provides an ideal platform to benchmark simulation results, as it is a multi-nC, multi-GeV accelerator. We benefited from excellent support during these studies, and further experimental activities are planned in the near future. Additional support from the U.S. Department of Energy has also been secured to continue and strengthen this collaboration.

Transverse multi-bunch dynamic effects. Long-range wakefields generated by higher-order

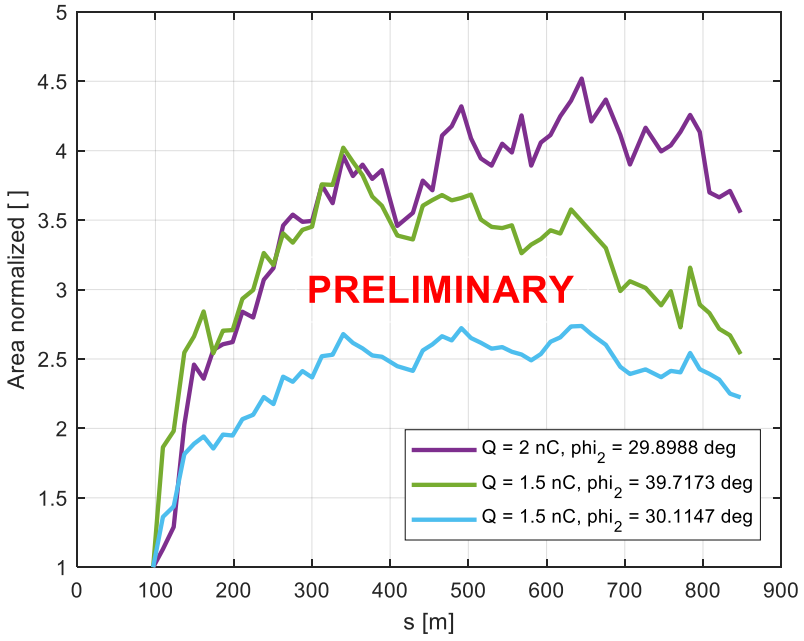

Figure 6: Ratio of the normalized areas measured along the FACET-II linac. Here, Q denotes the bunch charge and ϕ_2 represents the RF phase of the linac 2 varied in the measurements (the linac 1 and linac 3 phases are not varied during the measurements.

modes (HOMs) in accelerating structures can lead to bunch-to-bunch interactions and potentially drive beam break-up instabilities. To mitigate beam losses, these wakefields must be carefully suppressed through the RF design of the structures. The impact of such effects on beam stability is commonly quantified using the jitter amplification (JA), which measures the growth of transverse orbit jitter due to the defocusing action of transverse dipole modes.
To ensure stable operation of the high-energy linac, a design criterion has been established requiring the jitter amplification to remain below 1.1. Figure 7 illustrates the dependence of the jitter amplification on the transverse kick experienced by the following bunch, assuming an exponentially decaying wakefield affecting only subsequent bunches. The results indicate that maintaining the transverse kick below approximately 0.2 V/pC/mm/m satisfies the stability requirement. This constraint directly informs the RF design, in particular the choice of iris aperture. Once the RF structure is defined, the long-range transverse wake potential can be computed and used as input for beam dynamics simulations, for instance with the RF-Track code [1]. Figure 8 presents the resulting jitter amplification and transverse dipole wake function as a function of bunch spacing for a realistic set of higher-order modes. The results demonstrate that the jitter amplification remains below the acceptable threshold of 1.1 for bunch spacings greater than 5 ns, confirming the effectiveness of the wakefield suppression strategy.

RF Structure Optimization at 3 GHz. The study presents an updated design of 3 GHz traveling-wave accelerating structures for the FCC-ee high-energy injector linac, comparing two variants with average iris apertures of 0.12λ (baseline) and 0.13λ (alternative), building on earlier work [9]. Both 3 m-long structures are optimized for operation with 14.2 MW klystrons and incorporate tapered geometries to reduce wakefields and enhance multi-bunch stability. The baseline design achieves superior RF efficiency, reaching an average loaded gradient of 22.08 MV/m

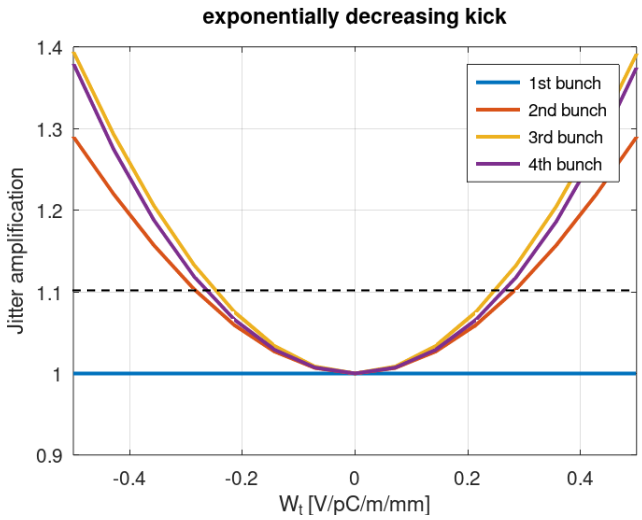

Figure 7: Transverse beam jitter amplification at the end of the high-energy linac as a function of the transverse kick acting on the linac. The dashed line indicates the acceptable limit of 1.1.

and a peak gradient of 79 MV/m, while the alternative reduces peak fields to 60 MV/m and surface power to 399 mW/μm^2 with only a slight reduction in gradient (21.15 MV/m). After RF pulse optimization, both structures demonstrate excellent beam-loading compensation, limiting energy variation across four bunches to about 0.06%. Detailed parameters are summarized in Table 3.

Table 3: Accelerating structure parameters for baseline and alternative structures

Parameter	Baseline (0.12λ)	Alternative (0.13λ)	Units
Frequency	3	3	GHz
Cell-to-cell Delta	1.4	1.4	mm
Entrance / Exit aperture	13.39 / 10.59	14.39 / 11.59	mm
Iris thickness	2.3 $\rightarrow$ 3.50	4.7 $\rightarrow$ 5.50	mm
Effective shunt impedance	107.24	96.90	MΩ/m
Klystron power	14.2	14.2	MW
Accelerating voltage	66.24	63.46	V
Average loaded gradient	22.08	21.15	MV/m
Peak instantaneous gradient	79	60	MV/m
Peak instantaneous surface power	624	399	mW/μm^2

Wakefield analyses, validated against ECHO2D simulations, confirm compliance with the transverse wakefield limit of 0.2 V/pC/mm/m for 25 ns bunch spacing, with flexibility down to 10 ns. The transverse wake potentials for both designs are illustrated in Figures 9 and 10. Sensitivity studies further show that geometric deviations up to 50 μm have minimal impact, although the cavity radius is the most critical parameter, leading to a recommended fabrication tolerance of ± 10 μm.

Energy and bunch compressors. The longitudinal requirements at booster injection are an rms energy spread of 0.1% and an rms bunch length of 4 mm. Since this bunch length is incompatible with propagation through the HE linac, and since on-crest operation is preferred to preserve emittance, an energy compressor (EC) has been implemented at the end of the HE

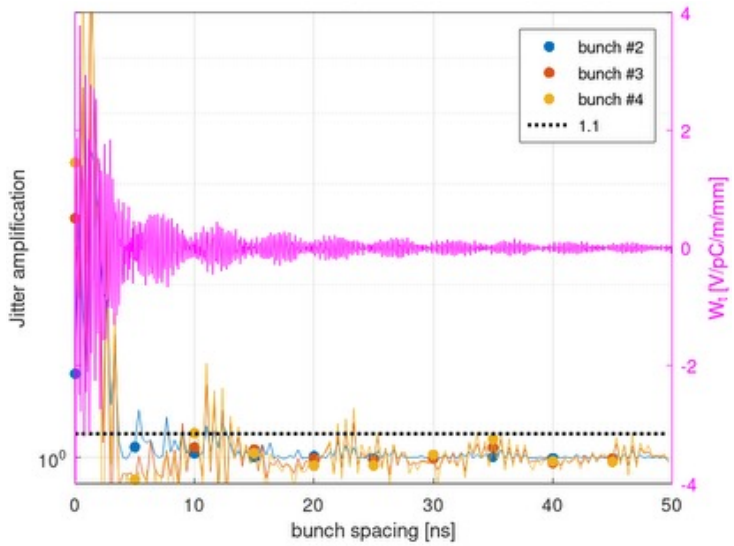

Figure 8: Transverse beam jitter amplification and transverse dipole wake function as a function of bunch spacing for a realistic distribution of higher-order modes. The dashed line indicates the acceptable limit of 1.1.

linac. A schematic representation of the system is shown in Figure 11, illustrating the layout of the energy compressor.

The EC provides several important advantages. It enables a modular injector design and decouples the HE linac from the booster constraints. It reduces the final energy spread at the linac end ($\sim 0.7\%$) down to the required 0.1%, while simultaneously decompressing the bunch to the 4 mm rms length required for injection into the booster. It also stabilizes the energy jitter, which is beneficial for beam transport through the transfer line in the presence of dispersion. The longer bunch length along the transfer line helps mitigate CSR effects. In addition, locating the EC at the end of the linac removes the need to install the 3 GHz RF system at a depth of approximately 250 m underground near the booster injection point.

The optimization of the EC at the previously considered RF frequency of 2.8 GHz has been discussed in detail elsewhere. A relatively moderate chicane with $R_{56} = 0.55$ m was selected, which is crucial for multi-bunch operation in order to keep the relative time delay between bunches within the specifications for booster injection. Using the chosen HE linac configuration and optimized EC parameters, simulations for a four-bunch train yield rms bunch lengths of about 4 mm and an rms energy spread of 0.1%, thus fulfilling the booster requirements. The selected EC configuration corresponds to a 3 GHz RF system with an integrated voltage of approximately 640 MV for multi-bunch operation.

Table 4: RF parameters and dipole angle and length for the EC.

f (GHz)	L_{str} (m)	a/λ	Integrated voltage (MV)	Angle (deg)	Length (m)
3	31.343	0.12	640	8.73	7.21

To ensure proper optics matching, two matching sections are required: one upstream of the chicane and another between the chicane and the RF section, allowing recovery of the FODO optics. Each matching section has a length of approximately 5 m, resulting in a total system length of about 100 m, including the matching sections, the chicane, and the RF modules.

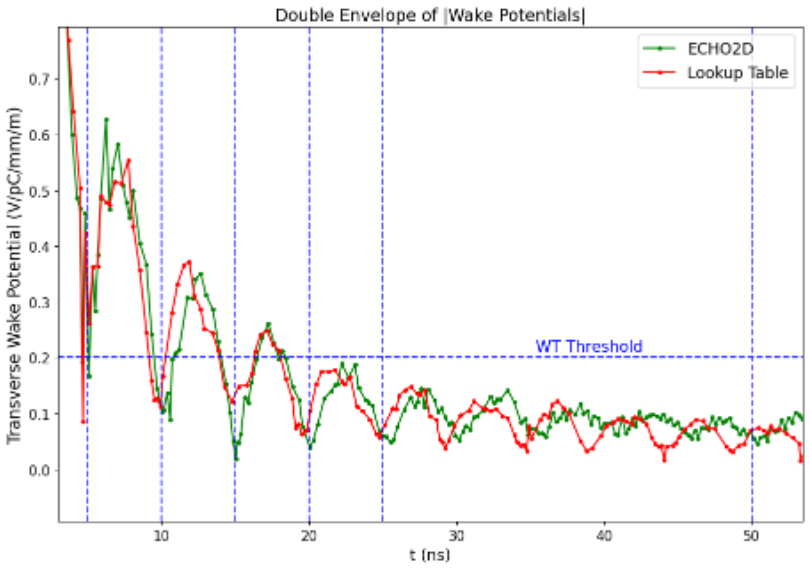

Figure 9: Envelope-of-the-envelope transverse wakefield potentials for the 0.12λ structure.

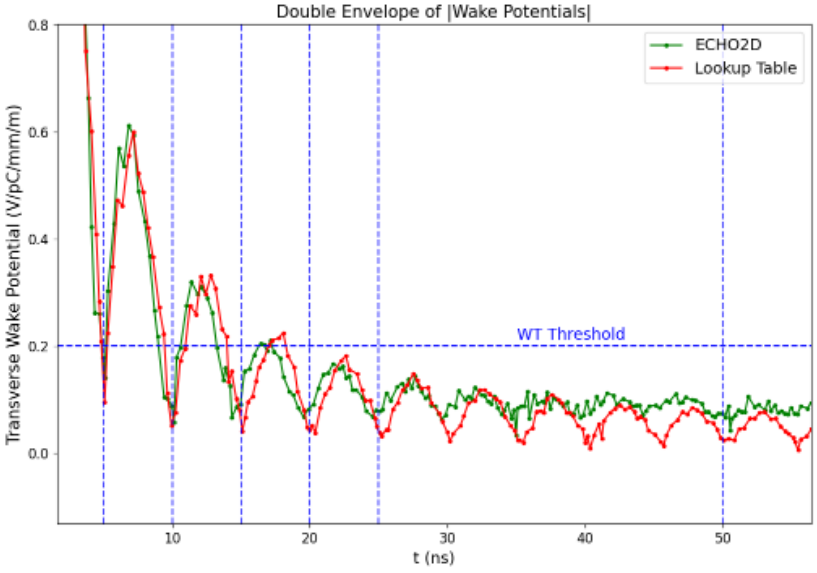

Figure 10: Envelope-of-the-envelope transverse wakefield potentials for the 0.13λ structure.

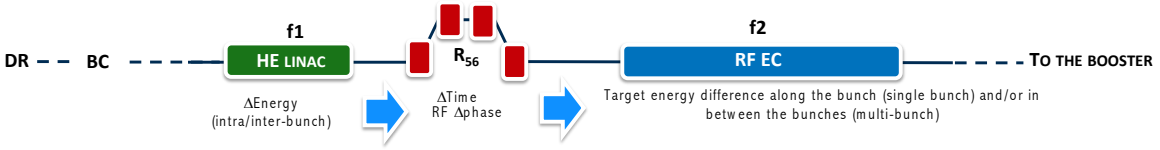

Figure 11: Schematic view of the EC.

Bunch compression is required to reduce the several-millimeter-long bunch delivered by the damping ring to the optimal length at the end of the high-energy (HE) linac. Previous studies have addressed this system [13], and further optimization of the bunch compressor (BC) is ongoing. In the present work, the existing baseline design has been adopted, the system has been dimensioned accordingly, and the beam has been properly matched at the entrance and exit of the energy compressor (EC). A schematic layout of the extraction section, including the damping ring and the bunch compressor region, is shown in Figure 12. The accelerating gradient in this section is still to be finalized. In this configuration, the integrated quadrupole strength is kept below 5 m^{-1}, and the optical functions are designed to maintain a relatively small Twiss parameter β at the fourth dipole magnet. This choice minimizes the impact of coherent synchrotron radiation (CSR), which has previously been estimated to induce an emittance growth of approximately 10% [13]. The current design provides a comfortable margin for the horizontal emittance, where most degradation is expected to occur. Further studies, including experimental validation, are planned to better quantify emittance growth and to refine the beam parameters.

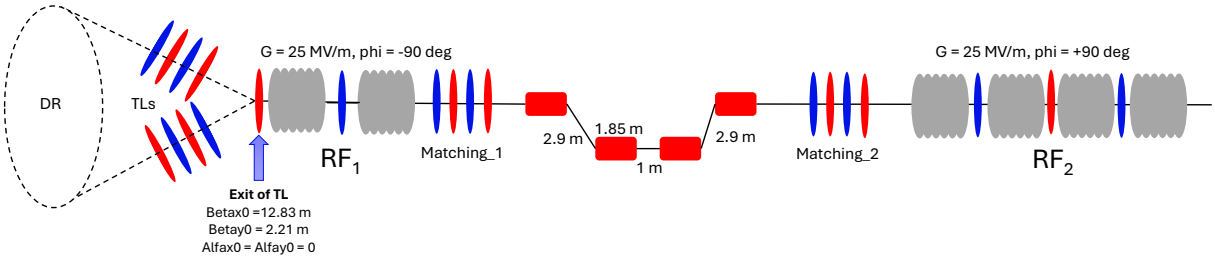

Figure 12: Schematic view of the bunch compressor (BC) region, including the extraction section from the damping ring. The accelerating gradient in this section is to be defined.

In conclusion, the WP1 studies demonstrate that the proposed HE linac design fulfills all requirements in terms of emittance preservation, stability, and multi-bunch operation, with significant performance margins. The selected configuration represents a robust and flexible baseline for the FCC-ee injector.

WP2: Electron Source – Summary of Activities and Results

WP2 focuses on the development of an electron source for the FCC-ee injector, addressing bunch generation, pulse-to-pulse charge modulation, and beam quality preservation. Progress has been achieved across all tasks, combining beam dynamics simulations, theoretical studies, and hardware development carried out jointly by CERN and PSI. The activities are structured such that the experimental validation (Task 4) will build upon the outcomes of Tasks 2 and 3.

Task 1 is dedicated to the evaluation of electron gun technologies and the corresponding beam dynamics optimization. A thermionic gun-based solution is currently under investigation, driven by CERN, based on a 300 kV DC gun followed by subharmonic bunching and S-band acceleration. This approach offers a simpler and more robust system by avoiding the complexity of laser and photocathode infrastructure, following concepts successfully implemented in previous facilities such as LEP at CERN and SLS at PSI. The study is currently at the proof-of-principle stage and aims to demonstrate that such a system can meet the beam requirements of the in-

jector chain. The reference configuration assumes the emission of 5 nC bunches with an initial bunch length of 1 ns from a 300 kV gun. The beam is compressed using a two-stage bunching system before injection into a 3 GHz travelling-wave accelerating structure, where acceleration and phase-space freezing occur. The overall layout of the bunching system is shown in Fig. 13. The first bunching stage operates at 250 MHz and introduces the required energy modulation

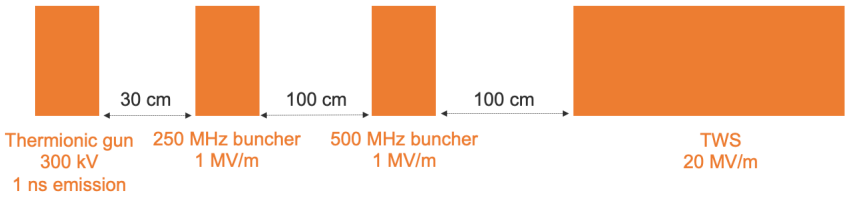

Figure 13: Schematic layout of the bunching system for the DC thermionic gun option.

for velocity bunching. However, this process also generates nonlinear distortions in the longitudinal phase space. To compensate for these effects, a second buncher operating at 500 MHz is placed at the point where the bunch has compressed to approximately half of its initial length. This second stage corrects the nonlinearities and significantly improves the phase-space quality, enabling further compression. The evolution of the longitudinal phase space along the bunching system is illustrated in Fig. 14. With this configuration, the beam can be compressed to ap-

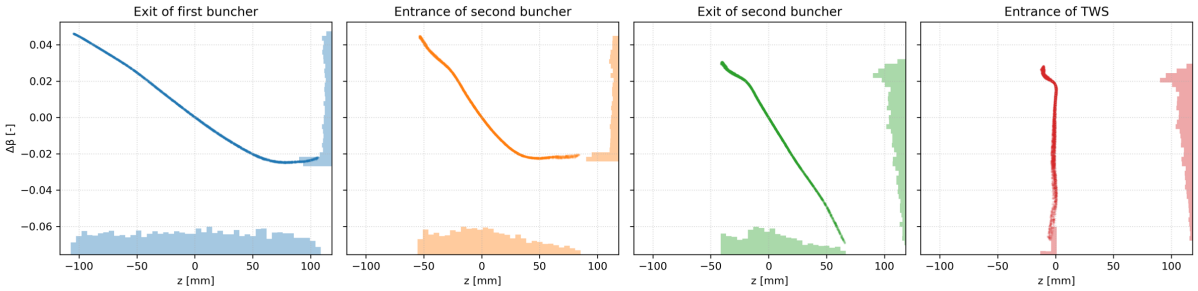

Figure 14: Evolution of the longitudinal phase space along the bunching system, showing compensation of nonlinear distortions.

proximately 1 mm rms bunch length at the entrance of the travelling-wave structure, meeting the requirements for subsequent acceleration. The results demonstrate that the thermionic gun approach is a viable alternative to the photogun solution, offering a simpler implementation while maintaining acceptable beam quality.

In parallel, the SwissFEL RF photogun remains the baseline option and is being studied collaboratively by PSI and CERN. These studies incorporate realistic hardware constraints and focus on the influence of the initial laser pulse shape on the beam dynamics. The results are essential to assess the feasibility of charge modulation techniques, including the use of deformable mirrors or fast iris systems, ensuring flexibility in the photogun-based solution.

Task 2 addresses the development of the experimental infrastructure and laser system for the electron source test facility. PSI has initiated the procurement of the laser system and other long lead-time components, while advancing the conceptual design of the source. Particular emphasis is placed on the laser injection scheme, which must deliver high pulse energy and large

transverse spot sizes compatible with the generation of 5 nC bunches. Complementary studies at CERN focus on charge emission limitations due to quantum efficiency (QE) effects at high laser intensities. A new model describing the QE dependence on laser pulse energy has been developed, enabling improved predictions of achievable charge from copper cathodes and guiding the system design. This work will be extended to semiconductor cathodes in future studies.

Task 3 concentrates on cathode handling and exchange systems to ensure operational compatibility between CERN and PSI. A cathode transfer and exchange mechanism is being designed at CERN, with support from PSI, to allow reliable and efficient operation across facilities. In parallel, PSI has completed the design review of the load-lock system for the test stand, initiated procurement procedures, and is investigating suitable caesium sources for cathode preparation.

In summary, WP2 has made significant progress in both baseline and alternative electron source concepts. The photogun solution continues to be refined with realistic constraints and advanced modeling, while the thermionic gun study provides a promising fallback option. Concurrent developments in laser systems, cathode handling, and infrastructure ensure that the experimental validation phase can proceed on a solid technical basis.

WP3: Positron Linac – Beam Dynamics, Target System and P³ Experiment

Positron Linac Study and DR acceptance

Over the past year, significant progress has been achieved in the study of the FCC-ee positron source, with a focus on the full production chain from the target to the damping ring (DR). The baseline configuration established in the FCC Feasibility Study relies on a conventional scheme in which a 2.86 GeV electron drive beam impinges on a 15 mm tungsten target, followed by a capture system consisting of a matching device, a solenoid-based capture linac, a separator chicane, a positron linac, and an energy compression system (ECS) upstream of the DR [14]. This design was shown to meet FCC-ee requirements with margin, while highlighting the DR acceptance as a critical factor in determining the overall performance. A major milestone during this period was the validation of the start-to-end simulation framework used for positron source studies. The model, combining Geant4 for particle production and RF-Track for beam dynamics tracking, was benchmarked against experimental data from the SuperKEKB positron source [15]. The comparison included scans of key parameters such as the primary electron impact position, capture-section magnetic field, and RF phases. The excellent agreement observed for the positron yield after the capture section provides strong confidence in the simulation tools now used for FCC-ee design studies. Building on this validated framework, recent efforts have focused on estimating the positron yield accepted by the DR, which represents the most relevant performance metric. Several complementary approaches were developed, including direct tracking in the DR, reconstruction of an effective six-dimensional acceptance ("6D sphere"), and a machine-learning model trained to reproduce the DR acceptance behavior. The results for both the 2.86 GeV and 1.54 GeV DR designs are summarized in Tables 5 and 6.
The simulations indicate that, for the current parameters, less than 60% of the positrons are accepted by the 1.54 GeV DR, motivating ongoing efforts to improve the acceptance and increase the usable positron yield. The corresponding phase space at the end of the transfer line is shown

Table 5: Preliminary simulation results for the FCC-ee positron source with the 2.86 GeV damping ring. For quantities with three values, the order is: DR tracking / 6D-sphere / ML model.

Parameter	**DR 2.86 GeV**
Yield before / after chicane / S1 / S2 / TL	4.20 / 3.85 / 3.63 / 3.40 / 3.27
Normalized emittance x/y @ S2 [mm·mrad]	15.13 / 14.31
Energy spread @ S2 [%]	5.8
Bunch length @ S2 [mm]	6.51
Yield @ TL (longitudinal cut)	2.07
Yield (6D sphere / ML)	1.00 / 1.31
Yield (DR tracking)	1.33
Beam size x/y [mm]	1.70/1.57 / 1.99/1.95 / 1.98/1.90
Normalized emittance x/y [mm·rad]	4.85/6.03 / 5.15/7.96 / 5.16/7.64
Geometric emittance x/y [μm]	0.87/1.08 / 0.92/1.42 / 0.92/1.37
Energy spread [%]	0.18 / 0.23 / 0.30
Bunch length [mm]	3.40 / 8.32 / 9.44

Table 6: Preliminary simulation results for the FCC-ee positron source with the 1.54 GeV damping ring. For quantities with three values, the order is: DR tracking / 6D-sphere / ML model.

Parameter	**DR 1.54 GeV**
Yield before / after chicane / S1 / S2 / TL	4.20 / 3.85 / 3.63 / 3.44 / 3.35
Normalized emittance x/y @ S2 [mm·mrad]	14.29 / 13.82
Energy spread @ S2 [%]	5.0
Bunch length @ S2 [mm]	5.17
Yield @ TL (longitudinal cut)	3.12
Yield (6D sphere / ML)	1.89 / 1.96
Yield (DR tracking)	1.94
Beam size x/y [mm]	3.19/2.60 / 3.57/2.99 / 3.54/3.02
Normalized emittance x/y [mm·mrad]	7.86/6.84 / 8.02/7.35 / 7.82/7.53
Geometric emittance x/y [μm]	2.61/2.27 / 2.66/2.44 / 2.60/2.50
Energy spread [%]	0.40 / 0.62 / 0.57
Bunch length [mm]	6.41 / 10.60 / 10.04

in Fig. 15, together with the projection of the DR acceptance. In parallel, studies have progressed

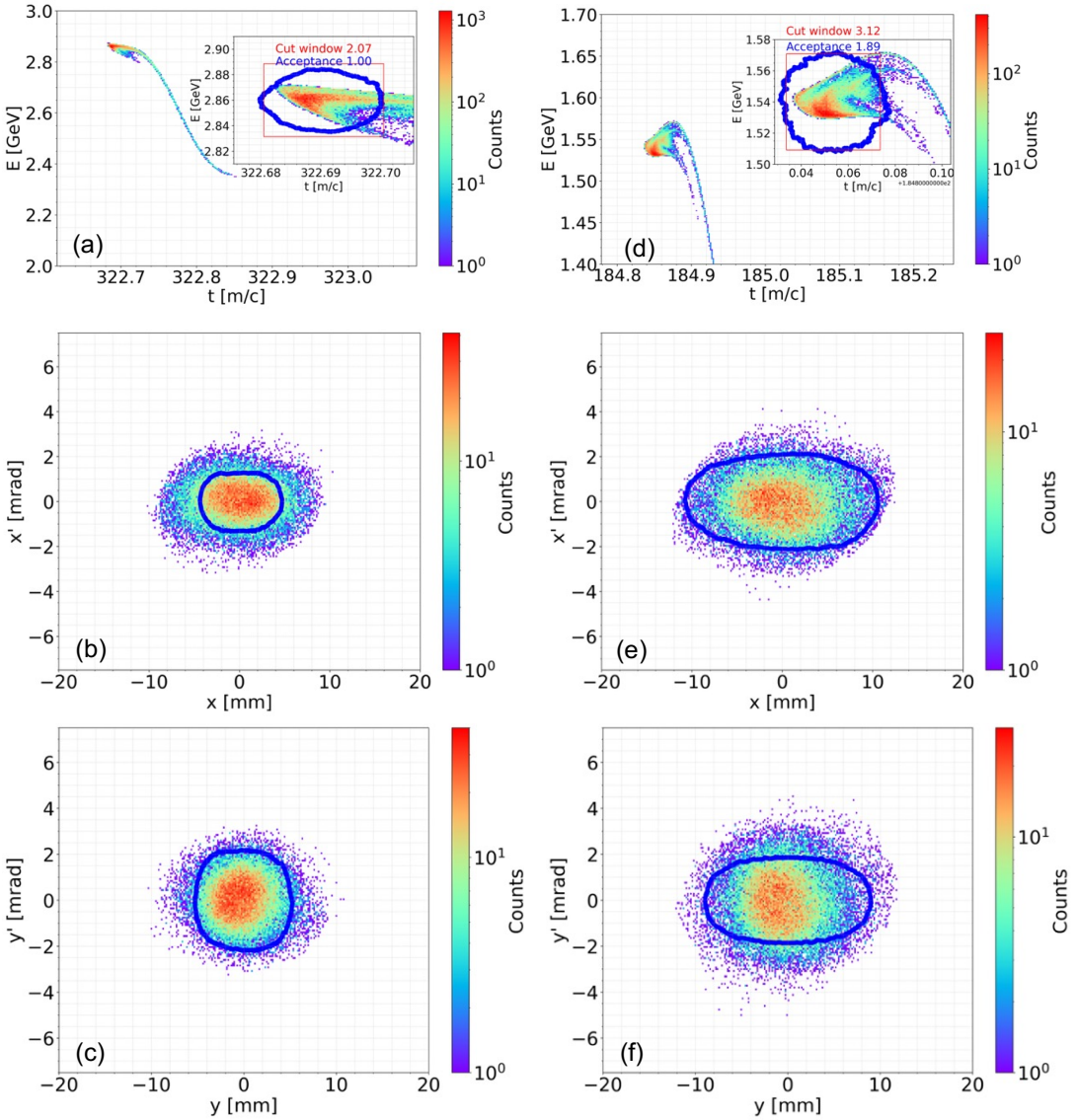

Figure 15: Positron phase space at the end of the transfer line for the 2.86 GeV (left) and 1.54 GeV (right) DR configurations. The projected DR acceptance is indicated.

toward possible upgrades of the capture system. In particular, a new approach based on 3 GHz S-band RF structures is being investigated, including traveling-wave (TW), standing-wave (SW), and hybrid (SW-TW) configurations. These studies also explore different focusing schemes, such as superconducting solenoid channels and downstream FODO lattices, with the aim of defining a realistic alternative baseline. The preliminary results are summarized in Table 7.

These studies show that different configurations offer trade-offs between yield, emittance, and energy spread. The ongoing effort aims to converge toward a solution that matches or improves the performance of the FCC FS baseline while remaining technically feasible. In addition, alternative schemes, including crystal-based positron production, have been investigated as part of exploratory studies [18].

Table 7: Preliminary simulation results for the 3 GHz positron capture system. S0 denotes the position after the second RF structure downstream of the chicane.

Configuration	**Gradient** [MV/m]	**Yield** @S0	**En. spread** [%]	**Emittance** [mm·mrad]	**Bunch length** [mm]
FS baseline	13.3	3.57	13.17	12.13/11.20	8.09
TW (1 T)	15	2.78	10.11	12.32/11.42	5.43
TW (0.5 T)	15	2.11	9.99	6.67/5.58	5.47
SW-TW (0.5 T)	18/15	1.95	12.44	6.34/6.20	5.83
SW (1 T)	18	2.85	13.05	9.47/9.50	6.02
SW (0.5 T)	18	2.11	12.63	5.81/5.69	6.17
TW (0.5 T FODO)	15	2.47	8.23	6.49/6.44	5.21

Status of the P³ Experiment

The PSI Positron Production (P³) project has reached key milestones during the reporting period. The full experimental setup has been installed in the SwissFEL tunnel, with the completion of the dedicated bunker in early 2026. Figure 16 illustrates the P³ experiment from concept through to installation at SwissFEL.

The 30-m long beamline installation is shown in Fig. 17 (left), while the RF system, including the klystron and modulator installations, is shown in Fig. 17 (right). The RF system is now ready to power the two accelerating structures, officially initiating high-power conditioning. First positron production is expected in summer 2026.

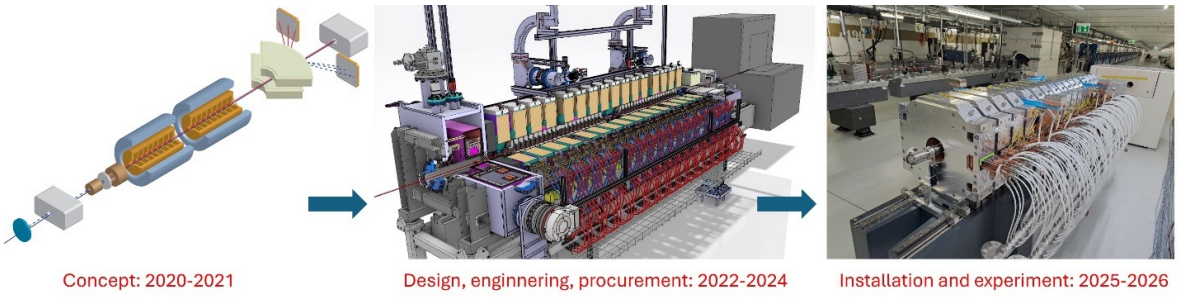

Figure 16: P³ experiment from concept to installation at SwissFEL.

In parallel, dedicated R&D activities have been carried out on target optimization and beam diagnostics. Studies of alternative target geometries, including conical designs, indicate potential improvements in positron yield and operational robustness [19].

A key component of the P³ experiment is the diagnostics system, which has been tested at the Beam Test Facility (BTF) at INFN-LNF using electron and positron beams with energies of 50–300 MeV. The goal of these measurements was to validate the performance of scintillator-based diagnostics for beam profile and charge measurements. While the scintillator screen measurements were not fully conclusive due to low charge density, the scintillator fiber system demonstrated high sensitivity and a clear linear response as a function of beam charge and energy. The fiber-based diagnostics also enabled reconstruction of the transverse beam profile through controlled scanning. Figure 18 shows an example of the scintillator signal as a function of the e^- and e^+ beam charge at a beam energy of 90 MeV. Further analysis is ongoing to refine calibration constants and quantify the system performance. These results confirm the viability of

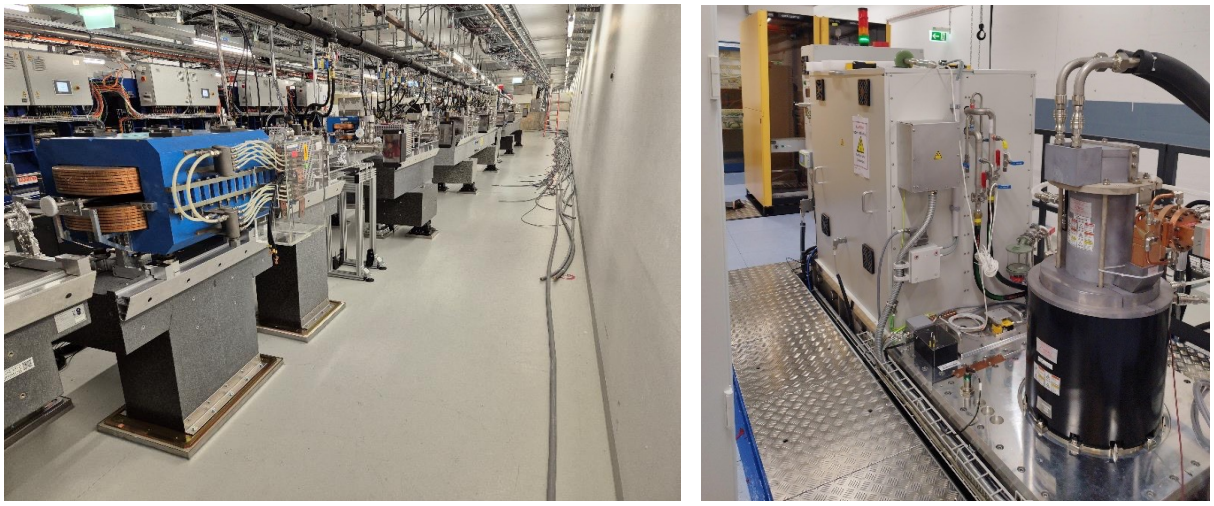

Figure 17: Left: P³ beamline installed in SwissFEL. Right: RF modulator in the technical gallery.

the P³ diagnostic approach and provide essential input for the upcoming experimental campaign.

Overall, the P³ project is progressing according to plan and is expected to deliver the first experimental validation of a high-yield positron source for the FCC-ee injector.

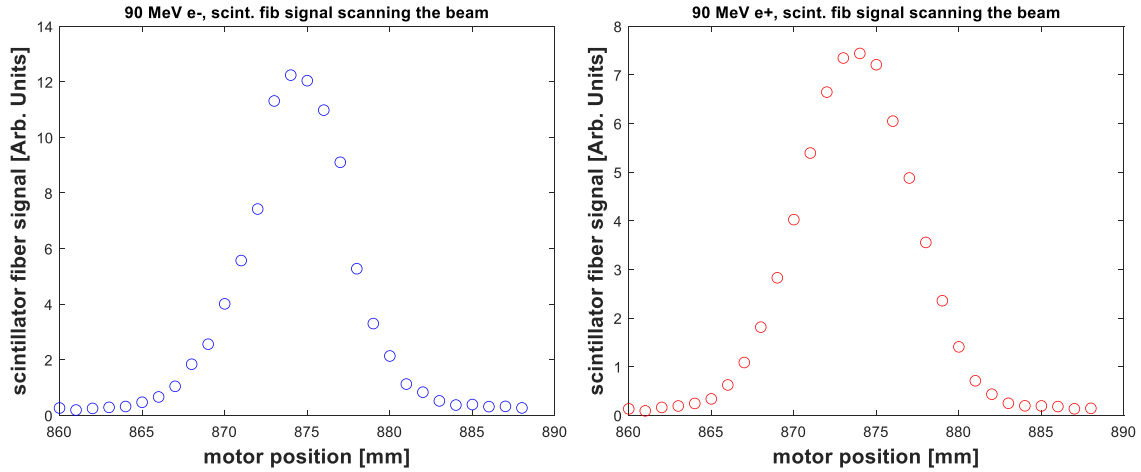

Figure 18: Calibration test at BTF: scintillator signal as a function of the e^- (left) and e^+ (right) beam charge at beam energy of 90 MeV.

WP4: Damping Ring and Transfer Lines – Summary of Activities and Results

The activities in 2025 focused on consolidating the FCC-ee Damping Ring (DR) design based on the baseline requirements established in the feasibility study, with the goal of validating and refining the proposed solutions through detailed lattice optimization, beam dynamics simulations, and hardware considerations. The DR is required to deliver beams with low transverse emittance of about 1.8 nm·rad and controlled energy spread below 0.1%, while ensuring sufficient acceptance for stable injection into the Booster Ring. A lattice at 2.86 GeV has been developed, compatible with the injector staging scenario and polarized beam operation. The adopted ge-

ometry is a compact hexagonal ring consisting of six arcs and six straight sections, providing high symmetry and flexibility for the integration of RF systems, damping wigglers, and injection and extraction hardware. Two arc configurations have been investigated, namely the Ten-Bend (10B) structure from the feasibility baseline and a more recent Six-Bend Achromat (6BA) design. Both solutions achieve the required natural emittance, although they exhibit relatively long transverse damping times on the order of 14-17 ms. Tracking studies indicate that the dynamic aperture and momentum acceptance remain below the desired operational margins, pointing to the need for further nonlinear optimization. In parallel, beam stability and impedance modeling activities have been initiated, including detailed analysis of machine components to minimize beam coupling impedance and the development of a simulation framework based on Xsuite to study wakefield-driven effects such as microwave and transverse mode-coupling instabilities. First investigations of electron cloud formation suggest that critical densities may be reached, requiring further dedicated studies. The design of the transfer lines has also progressed, with particular emphasis on the extraction line, which incorporates a magnetic chicane for bunch compression, reducing the bunch length from approximately 5 mm to 1 mm to meet the requirements of the high-energy linac. Overall, the 2025 work confirms the feasibility of the baseline DR design while identifying key areas for improvement. Future efforts will focus on nonlinear optimization, error tolerance studies, collective effects, and further refinement of both the lattice and the compression system to enhance the performance and robustness of the FCC-ee injector complex.

WP5: Preparatory phase for the Technical Design Report

Under the new organizational structure of the FCC-ee Injector at CERN, the CHART collaboration, led by PSI, will play a key role in coordinating the beam physics study. In this context, and as a deliverable of the study, the functional specifications of the various subsystems comprising the injector complex will be defined in order to involve the technical teams at CERN and, where appropriate, at PSI, in defining the engineering specifications and any prototypes that will form an integral part of the Technical Design Report (TDR).
The definition and finalization of the layout, which will be referred to as the *reference design*, will enable the study of the injector's positioning on the CERN site and the launch of civil engineering studies for the buildings, with the consequent integration of the injector subsystems.

3 Conclusions and outlook

Even during the reorganization of the Fcc-ee Injector pillar at CERN following the Feasibility Study phase, the work carried out within WP1–WP4 has continued to significantly advance the design and validation of the FCC-ee injector complex over the past year. The studies performed so far confirm the feasibility of the baseline solutions for the linacs, sources, and positron production chain. Work is still ongoing to define the baseline configuration of the damping ring, with several options under consideration, particularly regarding positron acceptance and emittance damping.
Several important milestones have already been achieved. These include the adoption of a linac operating frequency of 3.006 GHz, enabling synchronisation with the booster and collider

frequencies. In addition, the installation of the P^3 experiment has been completed, and key components for the electron source test stand at PSI, such as the laser system and the lock-lock system for cathode replacement, have been ordered.
The progress achieved so far provides a solid foundation for the next phase of the project, which will focus on finalising the baseline design, improving system robustness, and preparing the Technical Design Report (TDR).
In parallel with the coordination of the beam physics design of the injector, PSI is responsible for the development, construction, installation, and testing of several subsystems and associated deliverables:

1. Design, construction, and testing of a prototype accelerating structure for the HE-linac (1.1), as well as an S-band RF pulse compressor (1.2), including validation and performance measurements. A key outcome will be the definition and documentation of the industrialisation process for large-scale production, ensuring cost-effective, efficient, and reproducible manufacturing of RF accelerating structures (1.3).

2. Installation, commissioning, and testing of the electron source, including verification of operational parameters and integration with the relevant injector subsystems (2).

3. Completion of the positron source installation at PSI and execution of the associated experimental programme, including system commissioning, data acquisition, and analysis (3).

Figure 19 provides an overview of the project timeline, highlighting the deliverables described above. Some activities are foreseen to extend until 2029 in order to ensure the completion of the scientific programme and the production of additional RF component prototypes.

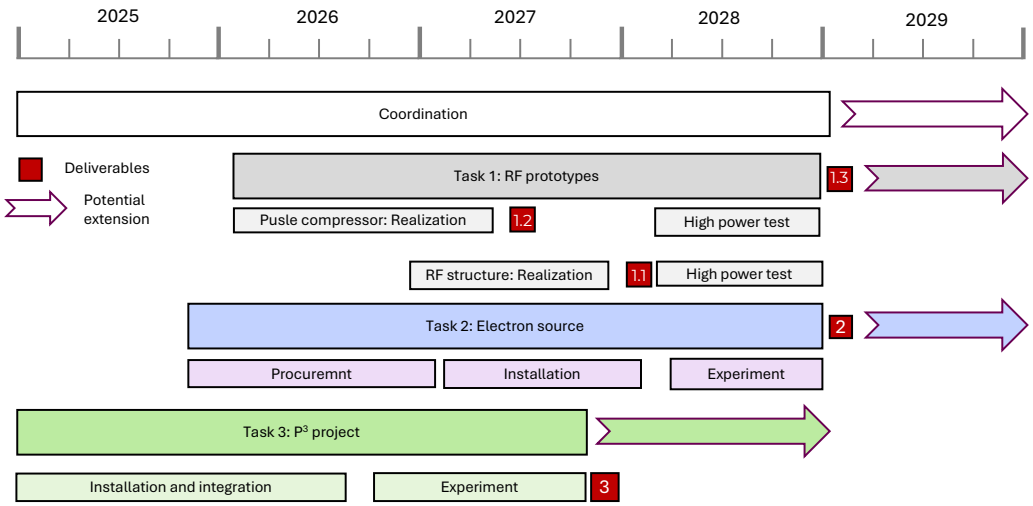

Figure 19: Timeline of key activities to be carried out at the PSI.

4 Publications and Outreach

Publications

- S. Bettoni, A. Latina, and A. Grudiev, "Transverse beam jitter damping along the FCC-ee injector linacs," Phys. Rev. Accel. Beams 28, 061601 (2025).
- A. Kurtulus et al., "RF design and optimization of the high-energy linac for the FCC-ee injector complex," Phys. Rev. Accel. Beams 28, 101601 (2025).
- F. Alharthi et al., "Modeling of the positron sources: Experiment-based benchmarking using SuperKEKB," Phys. Rev. Accel. Beams 28 (2025).
- F. Alharthi et al., "FCC-ee positron source from conventional to crystal-based," NIM A 1075 (2025)
- N. Vallis et al., "Conical targets for enhanced high-current positron sources," NIM B 568 (2025).

Conferences and workshops

- FCC Week 2025: An entire session devoted to studies of the FCC-ee injector, featuring 10 papers summarising the injector chapter of the FSR.
- A. Latina, "FCC-ee injector: Single and multibunch instability", eeFACT 2025
- T. Lucas, "Requirements for electron sources for lepton colliders", eeFACT 2025.
- P. Craievich, "Tuning-free high-gradient RF structures: From SwissFEL to FCC-ee - A scalable technology for future accelerators", NaPAC 2025.
- P. Craievich, Lecture on the FCC-ee Injector, International School of Particle Accelerators, Erice, Italy, 2025

PhD thesis

- Fahad Alharthi, "Design and validation studies of the FCC-ee positron source: from advanced simulations to proof-of-principle experiments at PSI", Accelerator Physics, Université Paris-Saclay, 2025.
- Adnan Kurtulus, "Impedance Studies of the HL-LHC Collimators & RF Design and Optimization of the Next-Generation Injector Linacs", Department of Information Technology and Electrical Engineering, ETH Zurich, 2026.

References

[1] A. Latina, *RF-Track v2.5.5*, Zenodo (2020), DOI: 10.5281/zenodo.3887084.

[2] A. Latina et al., "Experimental demonstration of a global dispersion-free steering correction," Phys. Rev. ST Accel. Beams 17, 042803 (2014).

[3] A. Latina, J. Pfingstner, D. Schulte, E. Adli, F. J. Decker, and N. Lipkowitz, "Experimental demonstration of a global dispersion-free steering correction at the new linac test facility at SLAC", Phys. Rev. ST Accel. Beams 17, 042803 (2014) - Published 11 April, 2014

[4] A. Latina et al., "Tests of wakefield-free steering at ATF2," Proc. IPAC2015.

[5] S. Bettoni, "Update on the FCC-ee injector" presented at the Cool Collider Workshop, Oct. 2024, Amsterdam, Netherlands, https://indico.slac.stanford.edu/event/9113/.

[6] A. Latina *et al.*, "Tests of wakefield-free steering at ATF2" in 5th Proc. Int. Particle Accelerator Conf. (IPAC'15), Richmond, US, May 2015, paper MOPJE059, pp. 438-441, doi:10.18429/JACoW-IPAC2015-MOPJE059.

[7] S. Bettoni, A. Latina, and A. Grudiev, "Transverse beam jitter damping along the FCC-ee injector linacs," Phys. Rev. Accel. Beams 28, 061601 (2025).

[8] A.Kurtulus, A. Grudiev, A. Latina, S. Bettoni, P. Craievich, and J.-Y. Raguin, "RF Design and 3D Modeling of a 3 GHz High-Energy Linac for the FCC-ee Injector", IPAC'26.

[9] A. Kurtulus et al., "RF design and optimization of the high-energy linac for the FCC-ee injector complex," Phys. Rev. Accel. Beams 28, 101601 (2025).

[10] S. Bettoni, "FCC-ee injector: linacs design for single- and multi-bunch effects", presented at FCC Week 2025, Wien, Austria, June 2025 https://indico.cern.ch/event/1408515/.

[11] A. Latina, "FCC-ee injector: Single and multibunch instability", eeFACT 2025

[12] CHART report 2024, https://chart.ch/.

[13] S. Spampinati, "Positron bunch and energy compressor (to/from damping ring)," FCC Week 2024.

[14] M. Benedikt et al., *Future Circular Collider Feasibility Study Report, Vol. 2.*

[15] F. Alharthi et al., "Modeling of the positron sources: Experiment-based benchmarking using SuperKEKB," Phys. Rev. Accel. Beams 28 (2025).

[16] M. Benedikt et al., "FCC-ee: The lepton collider," Eur. Phys. J. ST 228 (2019).

[17] Y. Wang et al., "FCC-ee positron capture system based on 3 GHz RF structures," Proceedings IPAC'26.

[18] F. Alharthi et al., "FCC-ee positron source from conventional to crystal-based," NIM A 1075 (2025).

[19] N. Vallis et al., "Conical targets for enhanced high-current positron sources," NIM B 568 (2025).